Journal of Computational and Applied Mathematics 234 (2010) 1904–1911

Contents lists available at ScienceDirect

Journal of Computational and Applied Mathematics

journal homepage: www.elsevier.com/locate/cam

Time-harmonic solution for acousto-elastic interaction with controllability and spectral elements

Sanna Mönkölä

Department of Mathematical Information Technology, University of Jyväskylä, P.O. Box 35 (Agora), FI-40014 University of Jyväskylä, Finland

ARTICLE INFO

Article history:
Received 14 December 2007
Received in revised form 25 March 2008

MSC:
74F10
65N30
65N35
93B05

Keywords:
Fluid-structure interaction
Acoustic waves
Elastic waves
Coupled problem
Time-harmonic solution
Spectral element method
Controllability
Conjugate gradient algorithm

ABSTRACT

The classical way of solving the time-harmonic linear acousto-elastic wave problem is to discretize the equations with finite elements or finite differences. This approach leads to large-scale indefinite complex-valued linear systems. For these kinds of systems, it is difficult to construct efficient iterative solution methods. That is why we use an alternative approach and solve the time-harmonic problem by controlling the solution of the corresponding time dependent wave equation.

In this paper, we use an unsymmetric formulation, where fluid-structure interaction is modeled as a coupling between pressure and displacement. The coupled problem is discretized in space domain with spectral elements and in time domain with central finite differences. After discretization, exact controllability problem is reformulated as a least-squares problem, which is solved by the conjugate gradient method.

1. Introduction

Acoustic waves are small oscillations of pressure, which are associated with local motions of particles in fluid domain Ω_f. The linear theory of elasticity models mechanical properties in structure Ω_s assuming small deformations. Acousto-elastic interaction between these two media constitutes a coupled problem. Several phenomena, such as seismic waves in the earth and ultrasonic waves used to detect flaws in materials, can be described by an acousto-elastic model. Two approaches, in which the displacement is solved in the elastic structure, predominate in modeling the interaction between acoustic and elastic waves. Expressing the acoustic wave equation by the velocity potential results in a symmetric system of equations (see, e.g., [1–4]), while using the pressure in the fluid domain leads to an unsymmetric formulation (see, e.g., [5–8]).

In this paper, we present the acousto-elastic interaction between pressure and displacement, and thereby concentrate on the unsymmetric approach. We formulate the time-harmonic acousto-elastic interaction as an exact controllability problem [9] via the corresponding time dependent system. The time dependent problem is discretized in space domain with the spectral element method (SEM) and in time domain with the second-order central finite differences. The combination of these discretization methods is well known with wave equations (see, e.g., [10]). The methods related to spectral elements are studied in the context of the time dependent acousto-elastic problem with second-order time-stepping schemes; see for instance Refs. [11,12,6].

After discretization, we solve the control problem by a conjugate gradient (CG) algorithm which is related to that developed in [13] for the acoustic wave equation. If an unpreconditioned CG algorithm is used, the number of iterations

E-mail address: sanna.monkola@jyu.fi.

0377-0427/$ – see front matter © 2009 Elsevier B.V. All rights reserved.
doi:10.1016/j.cam.2009.08.040

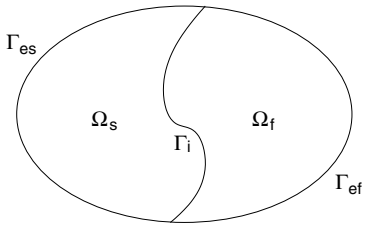

Fig. 1. The domain Ω is divided into the solid part Ω_s and the fluid part Ω_f.

grows rapidly with the order of spectral element [14]. That is why we use a modification of Kickinger's [15] algebraic multigrid (AMG), introduced in [16], for preconditioning the conjugate gradient algorithm.

The rest of this paper is organized as follows. First, the mathematical model is presented in Section 2. Then, we discretize the coupled problem in space domain with spectral elements in Section 3. For time discretization we use central finite differences in Section 4. In Section 5, we present the control problem and the preconditioned conjugate gradient algorithm. Finally, we show some numerical experiments in Section 6.

2. Mathematical model

We consider the use of a control algorithm to solve the time-harmonic acousto-elastic problem in the domain $\Omega \subset \mathbb{R}^2$, which is divided into the solid part Ω_s and the fluid part Ω_f by the interface Γ_i (see Fig. 1). Instead of solving directly the time-harmonic equation, we return to the corresponding time dependent equation (see, e.g., [17,10]) and look for time-periodic solution. The convergence is accelerated with a control technique by representing the original time-harmonic equation as an exact controllability problem [18,19] for the time dependent wave equation

$$\frac{1}{\rho_f(\mathbf{x})c(\mathbf{x})^2}\frac{\partial^2 p_f}{\partial t^2} - \nabla\cdot\left(\frac{1}{\rho_f(\mathbf{x})}\nabla p_f\right) = f, \quad \text{in } \Omega_f \times [0,T], \tag{1}$$

$$p_f = 0, \quad \text{on } \Gamma_{0f} \times [0,T], \tag{2}$$

$$\frac{1}{c(\mathbf{x})}\frac{\partial p_f}{\partial t} + \frac{\partial p_f}{\partial \mathbf{n}_f} = y_{\text{ext}}, \quad \text{on } \Gamma_{\text{ef}} \times [0,T], \tag{3}$$

$$\rho_f(\mathbf{x})\frac{\partial^2 \mathbf{u}_s}{\partial t^2}\cdot\mathbf{n}_s - \frac{\partial p_f}{\partial \mathbf{n}_f} = 0, \quad \text{on } \Gamma_{\text{i}} \times [0,T], \tag{4}$$

$$\rho_s(\mathbf{x})\frac{\partial^2 \mathbf{u}_s}{\partial t^2} - \nabla\cdot\sigma(\mathbf{u}_s) = \mathbf{f}, \quad \text{in } \Omega_s \times [0,T], \tag{5}$$

$$\mathbf{u}_s = 0, \quad \text{on } \Gamma_{0s} \times [0,T], \tag{6}$$

$$\rho_s(\mathbf{x})\mathbf{B}\frac{\partial \mathbf{u}_s}{\partial t} + \sigma(\mathbf{u}_s)\mathbf{n}_s = \mathbf{g}_{\text{ext}}, \quad \text{on } \Gamma_{\text{es}} \times [0,T], \tag{7}$$

$$\sigma(\mathbf{u}_s)\mathbf{n}_s - p_f\mathbf{n}_f = 0, \quad \text{on } \Gamma_{\text{i}} \times [0,T], \tag{8}$$

where f, y_{ext}, $\mathbf{f}$, and $\mathbf{g}_{\text{ext}}$ are the source terms. Length of the time interval is marked as T, p_f denotes the pressure, and $\mathbf{u}_s = (\mathbf{u}_{s1}, \mathbf{u}_{s2})^{\text{T}}$ is the displacement field depending on the spatial variable $\mathbf{x} = (x_1, x_2)^{\text{T}} \in \mathbb{R}^2$. Coefficients $\rho_f(\mathbf{x})$ and $\rho_s(\mathbf{x})$ represent the densities of media in domains Ω_f and Ω_s, respectively, and $c(\mathbf{x})$ is the speed of sound in fluid domain. The stress tensor is expressed as $\sigma(\mathbf{u}_s) = \rho_s(\mathbf{x})\left(c_p(\mathbf{x})^2 - 2c_s(\mathbf{x})^2\right)(\nabla\cdot\mathbf{u}_s)\mathbb{1} + 2\rho_s(\mathbf{x})c_s(\mathbf{x})^2\epsilon(\mathbf{u}_s)$ with the speed of the pressure wave $c_p(\mathbf{x})$, the speed of the shear wave $c_s(\mathbf{x})$, the identity matrix $\mathbb{1}$, and the linearized strain tensor $\epsilon = \frac{1}{2}\left(\nabla\mathbf{u}_s + (\nabla\mathbf{u}_s)^{\text{T}}\right)$. The outward normal vectors to domains Ω_f and Ω_s are marked as $\mathbf{n}_f = (n_{f1}, n_{f2})^{\text{T}}$ and $\mathbf{n}_s = (n_{s1}, n_{s2})^{\text{T}}$.

The fluid domain is bounded by $\Gamma_{\text{f}} = \Gamma_{0\text{f}} \bigcup \Gamma_{\text{ef}} \bigcup \Gamma_{\text{i}}$, and $\Gamma_{\text{s}} = \Gamma_{0\text{s}} \bigcup \Gamma_{\text{es}} \bigcup \Gamma_i$ constitutes the boundary for the solid domain Ω_s. The boundaries $\Gamma_{0\text{f}}$ and $\Gamma_{0\text{s}}$ are assumed to be rigid, whereas on the artificial boundaries Γ_{ef} and Γ_{es} we impose the conventional first-order absorbing boundary conditions [20,21], where $\mathbf{B}$ is a symmetric positive definite 2×2-matrix defined by

$$\mathbf{B} = \begin{pmatrix} c_p(\mathbf{x})n_{s1}^2 + c_s(\mathbf{x})n_{s2}^2 & n_{s1}n_{s2}(c_p(\mathbf{x}) - c_s(\mathbf{x})) \\ n_{s1}n_{s2}(c_p(\mathbf{x}) - c_s(\mathbf{x})) & c_p(\mathbf{x})n_{s2}^2 + c_s(\mathbf{x})n_{s1}^2 \end{pmatrix}.$$

In addition to the system (1)–(8), we take into account the initial conditions $\mathbf{e} = (\mathbf{e}_0, \mathbf{e}_1)^{\text{T}}$ such that $\mathbf{e}_0 = (\mathbf{e}_{0f}, \mathbf{e}_{0s})^{\text{T}}$ and $\mathbf{e}_1 = (\mathbf{e}_{1f}, \mathbf{e}_{1s})^{\text{T}}$, and

$$p_f(\mathbf{x}, 0) = \mathbf{e}_{0f}, \quad \frac{\partial p_f}{\partial t}(\mathbf{x}, 0) = \mathbf{e}_{1f}, \quad \text{in } \Omega_f, \tag{9}$$

$$\mathbf{u}_s(\mathbf{x}, 0) = \mathbf{e}_{0s}, \quad \frac{\partial \mathbf{u}_s(\mathbf{x}, 0)}{\partial t} = \mathbf{e}_{1s}, \quad \text{in } \Omega_s. \tag{10}$$

For existence and uniqueness of the solution for the problem (1)–(10), we refer to [22], and for the corresponding time-harmonic problem to [23].

3. Spatial discretization

For space discretization, we use the spectral elements method (see, e.g., [24,17,6,10]), which is based on the weak formulation of the system (1)–(8). That is why we introduce the function spaces V and $\mathbf{V}$ by

$$V = \{v \in H^1(\Omega) \text{ such that } v = 0 \text{ on } \Gamma_{0f}\}, \tag{11}$$

$$\mathbf{V} = \{\mathbf{v} \in H^1(\Omega) \times H^1(\Omega) \text{ such that } \mathbf{v} = 0 \text{ on } \Gamma_{0s}\}. \tag{12}$$

Multiplication of the Eq. (1) with any test function v in the space V, and (5) with any test function $\mathbf{v}$ in the space $\mathbf{V}$, and use of the Green's formula result in the following weak formulation:

Find $(p_f, \mathbf{u}_s)$ satisfying $(p_f(t), \mathbf{u}_s(t)) \in (V \times \mathbf{V})$ for any $t \in [0, T]$ and

$$a_f(p_f, v) - \int_{\Gamma_i} \frac{\partial^2 \mathbf{u}_s}{\partial t^2} \cdot \mathbf{n}_s v \, ds = f_f(v), \tag{13}$$

$$a_s(\mathbf{u}_s, \mathbf{v}) - \int_{\Gamma_i} p_f \mathbf{n}_f \cdot \mathbf{v} \, ds = \mathbf{f}_s(\mathbf{v}), \tag{14}$$

for any $(v, \mathbf{v}) \in (V \times \mathbf{V})$ and $t \in [0, T]$ with

$$a_f(p_f, v) := \int_{\Omega_f} \frac{1}{\rho_f(\mathbf{x}) c(\mathbf{x})^2} \frac{\partial^2 p_f}{\partial t^2} v \, dx + \int_{\Omega_f} \frac{1}{\rho_f(\mathbf{x})} \nabla p_f \cdot \nabla v \, dx + \int_{\Gamma_{ef}} \frac{1}{c(\mathbf{x}) \rho_f(\mathbf{x})} \frac{\partial p_f}{\partial t} v \, ds, \tag{15}$$

$$f_f(v) := \int_{\Omega_f} f v \, dx + \int_{\Gamma_{ef}} \frac{1}{\rho_f(\mathbf{x})} y_{ext} v \, ds, \tag{16}$$

$$a_s(\mathbf{u}_s, \mathbf{v}) := \int_{\Omega_s} \rho_s(\mathbf{x}) \frac{\partial^2 \mathbf{u}_s}{\partial t^2} \cdot \mathbf{v} \, dx + \int_{\Omega_s} \sigma(\mathbf{u}_s) : \epsilon(\mathbf{v}) \, dx + \int_{\Gamma_{es}} \rho_s(\mathbf{x}) \mathbf{B} \frac{\partial \mathbf{u}_s}{\partial t} \cdot \mathbf{v} \, ds, \tag{17}$$

$$\mathbf{f}_s(\mathbf{v}) := \int_{\Omega_s} \mathbf{f} \cdot \mathbf{v} \, dx + \int_{\Gamma_{es}} \mathbf{g}_{ext} \cdot \mathbf{v} \, ds. \tag{18}$$

The computational domain Ω is divided into N_e quadrilateral elements Ω_i, $i = 1, \ldots, N_e$ such that $\Omega = \bigcup_{i=1}^{N_e} \Omega_i$. For the discrete formulation, we define the reference element $\Omega_{ref} = [0, 1]^2$ and affine mappings $\mathcal{G}_i : \Omega_{ref} \to \Omega_i$ such that $\mathcal{G}_i(\Omega_{ref}) = \Omega_i$. Then, the spectral element discretization is obtained from the weak formulation by restricting the problem defined in the infinite dimensional spaces V and $\mathbf{V}$ into finite dimensional subspaces V_h^r and $\mathbf{V}_h^r$. These discrete subspaces are given by $V_h^r = \{v_h \in V \text{ such that } v_h|_{\Omega_i} \circ \mathcal{G}_i \in Q^r\}$ and $\mathbf{V}_h^r = \{\mathbf{v}_h = (v_{h1}, v_{h2})^T \in \mathbf{V} \text{ such that } v_{hk}|_{\Omega_i} \circ \mathcal{G}_i \in Q^r, k = 1, 2\}$, where $Q^r(\Omega_i) = \{v(\xi, \zeta) = \sum_{p=0}^{r} \sum_{q=0}^{r} a_{pq} \xi^p \zeta^q, \ a_{pq} \in \mathbb{R}\}$ is the set of Lagrange interpolation polynomials of order r in $\mathbb{R}^2$. In one space dimension, the nodes of the basis functions are placed at the rth order Gauss–Lobatto (GL) discretization points that are the zeroes of $x_1(1 - x_1)L_r'(2x_1 - 1)$, $x_1 \in [0, 1]$, where L_r' is the derivative of the rth degree Legendre polynomial L_r. The GL points in $\mathbb{R}^2$ are given by the tensor product of the one-dimensional GL points. The integrals in the weak form of the equation are evaluated with the corresponding Gauss–Lobatto quadrature formulas. This leads to the semi-discretized coupled problem

$$\mathcal{M} \frac{\partial^2 \mathbf{U}}{\partial t^2} + \mathcal{S} \frac{\partial \mathbf{U}}{\partial t} + \mathcal{K} \mathbf{U} = \mathcal{F}, \tag{19}$$

where $\mathbf{U}$ is the global vector containing the values of the displacement $\mathbf{u}_s(\mathbf{x}, t)$ and the pressure $p_f(\mathbf{x}, t)$ at time t at the Gauss–Lobatto points of the spectral element mesh. The entries of the matrices $\mathcal{M}$, $\mathcal{S}$, and $\mathcal{K}$, and the right hand side vector $\mathcal{F}$, are given by the formulas

$$\mathcal{M} = \begin{pmatrix} \mathcal{M}_s & 0 \\ \mathcal{A}_{fs} & \mathcal{M}_f \end{pmatrix}, \quad \mathcal{S} = \begin{pmatrix} \mathcal{S}_s & 0 \\ 0 & \mathcal{S}_f \end{pmatrix}, \quad \mathcal{K} = \begin{pmatrix} \mathcal{K}_s & \mathcal{A}_{sf} \\ 0 & \mathcal{K}_f, \end{pmatrix}, \quad \mathcal{F} = \begin{pmatrix} \mathcal{F}_s \\ \mathcal{F}_f \end{pmatrix}$$

where matrix and vector blocks $\mathcal{M}_s$, $\mathcal{S}_s$, $\mathcal{K}_s$, and $\mathcal{F}_s$ represent the elastic waves, $\mathcal{M}_f$, $\mathcal{S}_f$, $\mathcal{K}_f$, and $\mathcal{F}_f$ correspond to the fluid domain, and matrices $\mathcal{A}_{fs}$ and $\mathcal{A}_{sf}$ arise from the coupling between acoustic and elastic wave equations. Since $\mathcal{M}_s$ and $\mathcal{M}_f$ are diagonal matrices, the inverse of the lower diagonal block matrix $\mathcal{M}$ is easily computed, and explicit time stepping with central finite differences requires only matrix–vector multiplications.

4. Time discretization

The time discretization of the semi-discrete equation (19) is performed with the central finite differences (see, e.g., [10]). This method is second-order accurate with respect to the time step Δt and leads to an explicit time-stepping scheme. Both properties are essential for computational efficiency.

The time interval $[0, T]$ is divided into N time steps, each of size $\Delta t = T/N$. After replacing the time derivatives in the semi-discretized form (19) by the approximations

$$\frac{\partial \mathbf{U}^i}{\partial t} \approx \frac{\mathbf{U}^{i+1} - \mathbf{U}^{i-1}}{2\Delta t} \tag{20}$$

$$\frac{\partial^2 \mathbf{U}^i}{\partial t^2} \approx \frac{\mathbf{U}^{i+1} - 2\mathbf{U}^i + \mathbf{U}^{i-1}}{\Delta t^2}, \quad i = 0, \ldots, N, \tag{21}$$

and taking into account the initial conditions (9)-(10), we obtain the fully discrete state equation

$$\begin{pmatrix} \mathcal{I} & & & & & \\ \frac{1}{2}\mathcal{C} & \mathcal{M} & & & & \\ \mathcal{B} & \mathcal{C} & \mathcal{D} & & & \\ & \ddots & \ddots & \ddots & & \\ & & \mathcal{B} & \mathcal{C} & \mathcal{D} & \\ & & & \mathcal{B} & \mathcal{C} & \mathcal{D} \end{pmatrix} \begin{pmatrix} \mathbf{U}^0 \\ \mathbf{U}^1 \\ \vdots \\ \vdots \\ \mathbf{U}^N \\ \mathbf{U}^{N+1} \end{pmatrix} - \begin{pmatrix} \mathcal{I} & 0 \\ 0 & \Delta t\, \mathcal{B} \\ 0 & 0 \\ \vdots & \vdots \\ \vdots & \vdots \\ 0 & 0 \end{pmatrix} \begin{pmatrix} \mathbf{e}_0 \\ \mathbf{e}_1 \end{pmatrix} - \Delta t^2 \begin{pmatrix} 0 \\ \frac{1}{2}\mathcal{F}^0 \\ \mathcal{F}^1 \\ \vdots \\ \vdots \\ \mathcal{F}^N \end{pmatrix} = 0, \tag{22}$$

where $\mathbf{U}^i = (\mathbf{u}_s^i, {p_f}^i)^{\mathrm{T}}$ is the vector $\mathbf{U} = (\mathbf{u}_s, p_f)^{\mathrm{T}}$ at time $i\Delta t$, $\hat{\mathbf{U}} = (\mathbf{U}^0, \mathbf{U}^1, \ldots, \mathbf{U}^N, \mathbf{U}^{N+1})^{\mathrm{T}}$ contains the vectors $\mathbf{U}^i$, $\mathcal{F}^i$ is the vector $\mathcal{F}$ at $t = i\Delta t$, and $\mathbf{e}_0 = (\mathbf{e}_{0s}, \mathbf{e}_{0f})^{\mathrm{T}}$ and $\mathbf{e}_1 = (\mathbf{e}_{1s}, \mathbf{e}_{1f})^{\mathrm{T}}$ are the initial conditions. The matrix blocks $\mathcal{B}$, $\mathcal{C}$, and $\mathcal{D}$ are given by the formulas

$$\mathcal{B} = \begin{pmatrix} \mathcal{M}_s - \frac{\Delta t}{2}\mathcal{S}_s & 0 \\ \mathcal{A}_{\mathrm{fs}} & \mathcal{M}_f - \frac{\Delta t}{2}\mathcal{S}_f \end{pmatrix}, \tag{23}$$

$$\mathcal{C} = \begin{pmatrix} -2\mathcal{M}_s + \Delta t^2 \mathcal{K}_s & \Delta t^2 \mathcal{A}_{\mathrm{sf}} \\ -2\mathcal{A}_{\mathrm{fs}} & -2\mathcal{M}_f + \Delta t^2 \mathcal{K}_f \end{pmatrix}, \tag{24}$$

$$\mathcal{D} = \begin{pmatrix} \mathcal{M}_s + \frac{\Delta t}{2}\mathcal{S}_s & 0 \\ \mathcal{A}_{\mathrm{fs}} & \mathcal{M}_f + \frac{\Delta t}{2}\mathcal{S}_f \end{pmatrix}, \tag{25}$$

while $\mathcal{I}$ is the identity matrix.

5. Conjugate gradient algorithm

Essentially, the solution procedure of the exact controllability problem is similar to those presented for the Helmholtz equation in [19,25] and for the Navier equation in [26]. After discretization, the exact controllability problem is reformulated as a least-squares optimization problem

$$\min \frac{1}{2} \begin{pmatrix} \mathbf{U}^N - \mathbf{e}_0 \\ \frac{\partial \mathbf{U}^N}{\partial t} - \mathbf{e}_1 \end{pmatrix}^{\mathrm{T}} \mathcal{L} \begin{pmatrix} \mathbf{U}^N - \mathbf{e}_0 \\ \frac{\partial \mathbf{U}^N}{\partial t} - \mathbf{e}_1 \end{pmatrix}, \tag{26}$$

where we use a short notation $\mathcal{L}$ for the block-diagonal matrix containing the non-coupling terms of the matrices $\mathcal{K}$ and $\mathcal{M}$ such that $\mathcal{L} = \mathrm{diag}\left(\mathcal{K}_s, \mathcal{K}_f, \mathcal{M}_s, \mathcal{M}_f\right)$.

The minimization problem (26) is solved with a preconditioned conjugate gradient algorithm. Each conjugate gradient iteration requires computation of the gradient of the discretized least-squares functional, solution of a linear system with the block-diagonal preconditioner $\mathcal{L}$, and some matrix–vector operations. Computation of the gradient is an essential point of the method. By following the adjoint state technique (see, e.g., [25]), we obtain the gradient

$$\mathbf{g}(\mathbf{e}, \hat{\mathbf{U}}(\mathbf{e})) = \mathcal{L} \begin{pmatrix} \mathbf{e}_0 - \mathbf{U}^N \\ \mathbf{e}_1 - \frac{\partial \mathbf{U}^N}{\partial t} \end{pmatrix} + \begin{pmatrix} \mathbf{Z}^0 \\ \Delta t\, \mathcal{B}^{\mathrm{T}} \mathbf{Z}^1 \end{pmatrix}, \tag{27}$$

where $\mathbf{Z}^0$ and $\mathbf{Z}^1$ are solutions of the adjoint state equation at time $t = 0$ and $t = \Delta t$, respectively.

For preconditioning the algorithm, we use the algebraic multigrid (AMG) method [16] (see also [27,19]). As a smoother for the AMG we use the successive over relaxation (SOR) method with relaxation factor equal to 1.2. One iteration of the SOR is used as pre- and post-smoothing. Additionally, in the beginning of every multigrid iteration, four iterations of the SOR are used to smooth the solution initially. So called W-cycle [28] is utilized as a multigrid iteration until the residual norm of the solution is smaller than 10^{-6}.

6. Numerical experiments

In this section, we show some numerical results in order to validate the method discussed in previous sections. The material parameters in fluid domain are $\rho_f(\mathbf{x}) = 1.0$ and $c(\mathbf{x}) = 1.0$. In solid domain, we use the values $c_p(\mathbf{x}) = 6.20$, $c_s(\mathbf{x}) = 3.12$, and $\rho_s(\mathbf{x}) = 2.7$. Angular frequency ω is the same for both media, and throughout the tests we set the propagation direction $(-1,0)$ by the vector $\boldsymbol{\omega} = (\omega_1, \omega_2) = (-1, 0)\omega$. For test problems, we use the right hand side functions

$$f = \left(1 - \frac{1}{c(\mathbf{x})^2}\right) \omega^3 \sin(\boldsymbol{\omega} \cdot \mathbf{x}) \cos(\omega t),$$

$$\mathbf{f} = (0, 0)^{\mathrm{T}},$$

$$y_{\mathrm{ext}} = \rho_f(\mathbf{x})\omega \left(\boldsymbol{\omega} \cdot \mathbf{n}_f \cos(\boldsymbol{\omega} \cdot \mathbf{x}) - \frac{\omega}{c(\mathbf{x})} \sin(\boldsymbol{\omega} \cdot \mathbf{x})\right) \cos(\omega t),$$

$$\mathbf{g}_{\mathrm{ext}} = -\rho_s(\mathbf{x})\omega C_n \begin{pmatrix} \cos\left(\frac{\boldsymbol{\omega} \cdot \mathbf{x}}{c_p(\mathbf{x})}\right) \sin(\omega t) \\ \cos\left(\frac{\boldsymbol{\omega} \cdot \mathbf{x}}{c_s(\mathbf{x})}\right) \sin(\omega t) \\ \sin\left(\frac{\boldsymbol{\omega} \cdot \mathbf{x}}{c_p(\mathbf{x})}\right) \cos(\omega t) \\ \sin\left(\frac{\boldsymbol{\omega} \cdot \mathbf{x}}{c_s(\mathbf{x})}\right) \cos(\omega t) \end{pmatrix},$$

where

$$C_n = \begin{pmatrix} c_p(\mathbf{x})\mathbf{n}_{s1}^2 + c_s(\mathbf{x})\mathbf{n}_{s2}^2 & \mathbf{n}_{s1}\mathbf{n}_{s2}\left(c_p(\mathbf{x}) - c_s(\mathbf{x})\right) & c_p(\mathbf{x})\mathbf{n}_{s1}\omega & c_s(\mathbf{x})\mathbf{n}_{s2}\omega \\ \mathbf{n}_{s1}\mathbf{n}_{s2}\left(c_p(\mathbf{x}) - c_s(\mathbf{x})\right) & c_p(\mathbf{x})\mathbf{n}_{s2}^2 + c_s(\mathbf{x})\mathbf{n}_{s1}^2 & \left(c_p(\mathbf{x}) - 2\frac{c_s(\mathbf{x})^2}{c_p(\mathbf{x})}\right)\mathbf{n}_{s2}\omega & c_s(\mathbf{x})\mathbf{n}_{s1}\omega \end{pmatrix}.$$

According to the results reported in [25,26], we choose the length of time step, for a certain element order r, to reduce the temporal error to a lower level than the spatial error. These values are presented in Table 1. For each element order r, we construct square element meshes, which are matching on the interface Γ_i. Numerical experiments are carried out on an AMD Opteron 885 processor at 2.6 GHz, and iterations are continued until the stopping criterion $\varepsilon = 10^{-4}$ is reached.

Algorithm 1 Preconditioned CG algorithm

Initialize $\mathbf{e} = 0$.
Solve the state equation (22) with initial condition $\mathbf{e}$.
Solve the corresponding adjoint state equation.
Compute the gradient $\mathbf{g}(\mathbf{e}, \hat{\mathbf{U}}(\mathbf{e}))$.
Solve linear system with the preconditioner $\mathcal{L}\mathbf{w} = -\mathbf{g}$.
Set $\varsigma_0 = -(\mathbf{w}, \mathbf{g})$ and $\varsigma = \varsigma_0$.
repeat
  Solve the state equation (22) with initial condition $\mathbf{w}$ and $\mathcal{F} = 0$.
  Solve the corresponding adjoint state equation.
  Compute the gradient update $\hat{\mathbf{g}} = \mathbf{g}(\mathbf{w}, \hat{\mathbf{U}}(\mathbf{w}))$.
  Compute $\eta = \frac{\varsigma}{(\mathbf{w}, \hat{\mathbf{g}})}$.
  Update $\mathbf{e} = \mathbf{e} + \eta\mathbf{w}$ and $\mathbf{g} = \mathbf{g} + \eta\hat{\mathbf{g}}$.
  Solve linear system with the preconditioner $\mathcal{L}\hat{\mathbf{g}} = -\mathbf{g}$.
  Compute $\gamma = \frac{1}{\varsigma}$ and $\varsigma = -(\hat{\mathbf{g}}, \mathbf{g})$.
  Update $\gamma = \varsigma\gamma$ and $\mathbf{w} = \hat{\mathbf{g}} + \gamma\mathbf{w}$.
until $\sqrt{\frac{\varsigma}{\varsigma_0}} < \varepsilon$

Table 1
The ratio between time step and mesh stepsize for different element orders.

	Element order r		
	1	2	3
$\Delta t/h$	0.1250	0.0227	0.0101

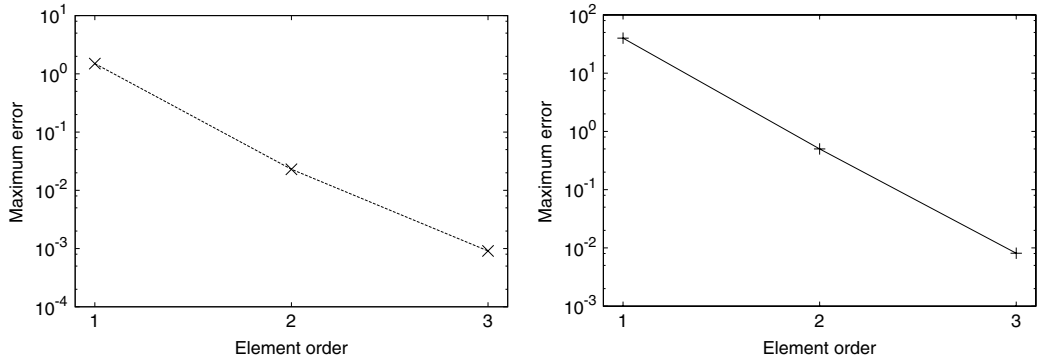

(a) Solid domain. (b) Fluid domain.

Fig. 2. Errors with respect to element order.

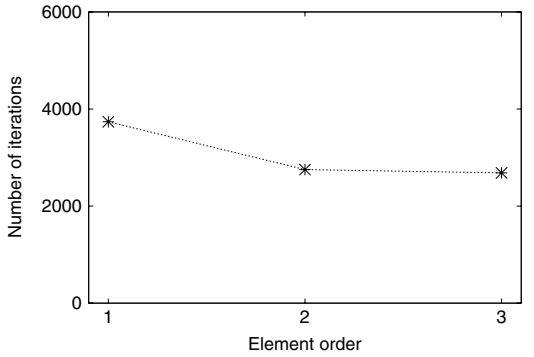

Fig. 3. Number of iterations with respect to element order.

6.1. Accuracy

The analytical solution of the first test problem is known to be

$$p_f = \omega\rho_f(\mathbf{x})\sin(\boldsymbol{\omega}\cdot\mathbf{x})\cos(\omega t),$$
$$\mathbf{u}_s = \begin{pmatrix}\cos(\boldsymbol{\omega}\cdot\mathbf{x}/c_p(\mathbf{x}))\cos(\omega t)\\ \cos(\boldsymbol{\omega}\cdot\mathbf{x}/c_s(\mathbf{x}))\cos(\omega t)\end{pmatrix}.$$

The problem is solved in a domain, which consists of the solid part $\Omega_s = [-1, 0] \times [0, 1]$ and the fluid part $\Omega_f = [0, 1] \times [0, 1]$. The coupling interface is set at $x_1 = 0$ for $x_2 \in [0, 1]$, and on the other boundaries we have the absorbing boundary conditions. Since there are no rigid boundaries, a modified preconditioner diag $\left(\mathcal{K}_s + \frac{\mathcal{M}_s}{10^4}, \mathcal{K}_f + \frac{\mathcal{M}_f}{10^4}, \mathcal{M}_s, \mathcal{M}_f\right)$ is used, instead of diag $\left(\mathcal{K}_s, \mathcal{K}_f, \mathcal{M}_s, \mathcal{M}_f\right)$, to avoid matrix singularities in preconditioning. Fig. 2 shows how the accuracy improves when element order grows with $\omega = 8\pi$ and $h = 1/20$. The number of iterations required to attain the stopping criterion was sufficiently large (see Fig. 3).

6.2. Scattering

This scattering test is solved in domain Ω, where the absorbing boundary coincides with the perimeter of the rectangle $[0, 5] \times [0, 3.75]$. In the center of the computational domain Ω, we have two rigid non-convex semi-open cavities. These reflectors are located at perpendicular distance of 1 from the absorbing boundary. Thus, the lower left corner of the left side cavity is at the point (1, 1) and the lower right corner of the right side cavity is at the point (4, 1). Internal width and

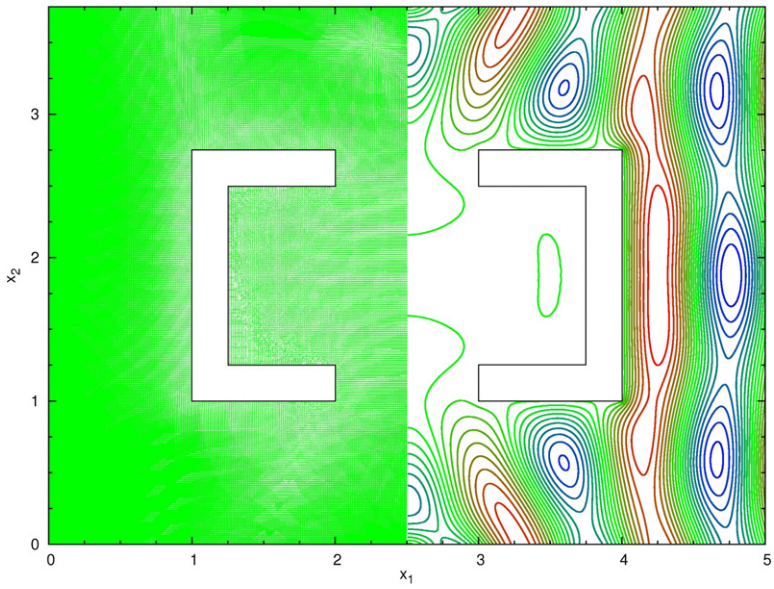

Fig. 4. Scattering solution with $r = 1, h = 1/80, \omega = 2\pi$.

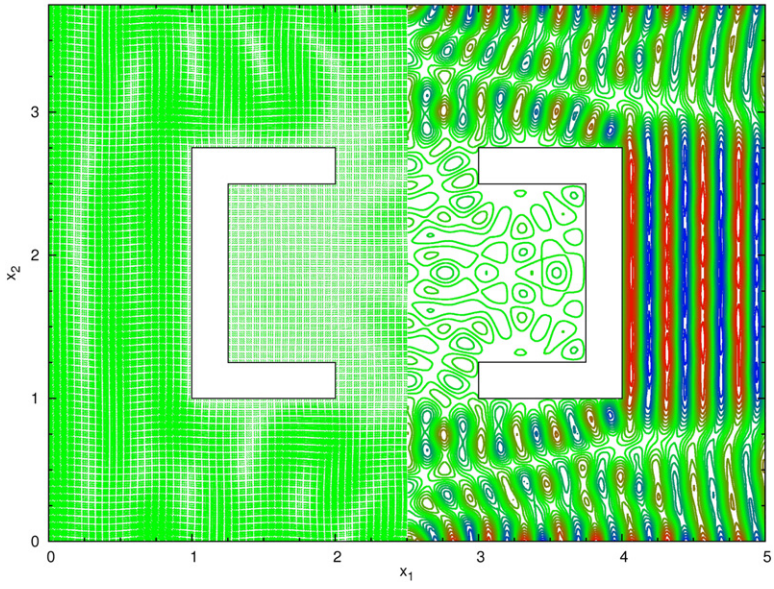

Fig. 5. Scattering solution with $r = 3, h = 1/20, \omega = 8\pi$.

height of each cavity are 0.75 and 1.25, respectively. Thickness of the wall is 0.25, and the distance between cavities is 1. The coupling interface is set at $x_1 = 2.5$ for $x_2 \in [0, 3.75]$. The left half of the domain Ω is set to be the solid domain Ω_s, and the right half of the domain Ω represents the fluid domain Ω_f. Two examples of scattering solutions are illustrated in Figs. 4 and 5, where displacements are presented as vector fields and pressures are presented as contours.

7. Conclusions

We considered the spectral element solution of time-harmonic acousto-elastic interaction problems by the exact controllability method. Simulation results show that the number of iterations required to attain the stopping criterion is large but independent of the element order. In future work, the central finite difference time discretization will be substituted by higher-order time discretization methods to reduce the number of iterations and improve the accuracy. Also symmetric fluid-structure interaction formulations, with coupling between velocity potential and displacement, will be discussed.

Acknowledgements

The author thanks Prof. Tuomo Rossi, Dr. Erkki Heikkola, and Dr. Timo Männikkö for useful advice and Dr. Janne Martikainen and MSc. Anssi Pennanen for providing the AMG solver.

References

[1] E. Chaljub, Y. Capdeville, J.-P. Vilotte, Solving elastodynamics in a fluid-solid heterogeneous sphere: A parallel spectral element approximation on non-conforming grids, Journal of Computational Physics 187 (2) (2003) 457–491.
[2] B. Flemisch, M. Kaltenbacher, B.I. Wohlmuth, Elasto-acoustic and acoustic-acoustic coupling on non-matching grids, International Journal for Numerical Methods in Engineering 67 (13) (2006) 1791–1810.
[3] L.G. Olson, K.J. Bathe, Analysis of fluid-structure interactions. A direct symmetric coupled formulation based on the fluid velocity potential, Computers & Structures 21 (1985) 21–32.
[4] L.L. Thompson, P.M. Pinsky, A space-time finite element method for structural acoustics in infinite domains, part I: Formulation, stability and convergence, Computer Methods in Applied Mechanics and Engineering 132 (1996) 195–227.
[5] A. Bermúdez, P. Gamallo, L. Hervella-Nieto, E. Rodríguez, Finite element analysis of pressure formulation of the elastoacoustic problem, Numerische Mathematik 95 (1) (2003) 29–51.
[6] D. Komatitsch, C. Barnes, J. Tromp, Wave propagation near a fluid-solid interface: A spectral-element approach, Geophysics 65 (2) (2000) 623–631.
[7] J. Mandel, M.O. Popa, Iterative solvers for coupled fluid-solid scattering, Applied Numerical Mathematics 54 (2) (2005) 194–207.
[8] X. Wang, K.-J. Bathe, Displacement/pressure based mixed finite element formulations for acoustic fluid-structure interaction problems, International Journal for Numerical Methods in Engineering 40 (11) (1997) 2001–2017.
[9] R. Glowinski, J.L. Lions, Exact and approximate controllability for distributed parameter systems (II), Acta Numerica (1995) 159–333.
[10] E. Zampieri, L.F. Pavarino, An explicit second order spectral element method for acoustic waves, Advances in Computational Mathematics 25 (4) (2006) 381–401.
[11] A. Cividini, A. Quarteroni, E. Zampieri, Numerical solution of linear elastic problems by spectral collocation methods, Computer Methods in Applied Mechanics and Engineering 104 (1) (1993) 49–76.
[12] E. Faccioli, F. Maggio, A. Quarteroni, A. Tagliani, Spectral domain decomposition methods for the solution of acoustic and elastic wave propagation, Geophysics 61 (1996) 1160–1174.
[13] M.O. Bristeau, R. Glowinski, J. Périaux, Using exact controllability to solve the Helmholtz equation at high wave numbers, in: R. Kleinman, T. Angell, D. Colton, F. Santosa, I. Stakgold (Eds.), Mathematical and Numerical Aspects of Wave Propagation, SIAM, Philadelphia, Pennsylvania, 1993, pp. 113–127.
[14] Y. Maday, A.T. Patera, Spectral element methods for the incompressible Navier-Stokes equations, in: A.K. Noor, J.T. Oden (Eds.), State-of-the-Art Surveys on Computational Mechanics, American Society of Mechanical Engineering, New York, 1989, pp. 71–143.
[15] F. Kickinger, Algebraic multigrid for discrete elliptic second-order problems, in: Multigrid Methods V, (Stuttgart, 1996), Springer-Verlag, Berlin, 1998, pp. 157–172.
[16] J. Martikainen, A. Pennanen, T. Rossi, Application of an algebraic multigrid method to incompressible flow problems, Reports of the Department of Mathematical Information Technology, Series B. Scientific Computing, B 2/2006, Department of Mathematical Information Technology, University of Jyväskylä (2006).
[17] D. Gottlieb, J.S. Hesthaven, Spectral methods for hyperbolic problems, Journal of Computational and Applied Mathematics 128 (1–2) (2001) 83–131.
[18] M.O. Bristeau, R. Glowinski, J. Périaux, Controllability methods for the computation of time-periodic solutions; Application to scattering, Journal of Computational Physics 147 (2) (1998) 265–292.
[19] E. Heikkola, S. Mönkölä, A. Pennanen, T. Rossi, Controllability method for the Helmholtz equation with higher-order discretizations, Journal of Computational Physics 225 (2) (2007) 1553–1576.
[20] B. Engquist, A. Majda, Radiation boundary conditions for acoustic and elastic wave calculations, Communications on Pure and Applied Mathematics 32 (1979) 313–357.
[21] A. Quarteroni, T. Tagliani, E. Zampieri, Generalized Galerkin approximations of elastic waves with absorbing boundary conditions, Computer Methods in Applied Mechanics and Engineering 163 (1998) 323–341.
[22] X. Feng, P. Lee, Y. Wei, Mathematical analysis of a fluid-solid interaction problem, Applicable Analysis 80 (3) (2001) 409–429.
[23] P. Cummings, X. Feng, Domain decomposition methods for a system of coupled acoustic and elastic Helmholtz equations, in: Proceedings of the Eleventh International Conference on Domain Decomposition Methods, DDM.org, 1999, pp. 203–210.
[24] G. Cohen, Higher-Order Numerical Methods for Transient Wave Equations, Springer-Verlag, Berlin, 2001.
[25] E. Heikkola, S. Mönkölä, A. Pennanen, T. Rossi, Controllability method for acoustic scattering with spectral elements, Journal of Computational and Applied Mathematics 204 (2) (2007) 344–355.
[26] S. Mönkölä, E. Heikkola, A. Pennanen, T. Rossi, Time-harmonic elasticity with controllability and higher order discretization methods, Journal of Computational Physics.
[27] T. Airaksinen, E. Heikkola, A. Pennanen, J. Toivanen, An algebraic multigrid based shifted-Laplacian preconditioner for the Helmholtz equation, Journal of Computational Physics 226 (2007) 1196–1210.
[28] W. Hackbusch, Multigrid Methods and Applications, Springer-Verlag, Berlin, Germany, 1985.